GPS Solutions (2021) 25:140
https://doi.org/10.1007/s10291-021-01177-0

ORIGINAL ARTICLE

Full-ISL clock offset estimation and prediction algorithm for BDS3

Junyang Pan[1,2] · Xiaogong Hu[1,3] · Shanshi Zhou[1,3] · Chengpan Tang[1,3] · Dongxia Wang[4] · Yufei Yang[4] · Wenli Dong[1]

Received: 21 August 2019 / Accepted: 27 August 2021 / Published online: 9 September 2021

Abstract
The Ka-band dual one-way measurements from Inter-Satellite Link (ISL) devices equipped on the third-generation Beidou Navigation Satellite System (BDS3) follow a time division multiple access (TDMA) structure and can calculate inter-satellite and satellite-ground clock offsets. L-band two-way satellite time and frequency transfer (TWSTFT) is also applied for time synchronization between satellites and ground master. We focus on a full-ISL clock offset estimation and prediction algorithm that estimates all satellite clock parameters simultaneously utilizing ISL clock observations and also synchronizes the constellation to the system time in Beidou Time (BDT) using Ka-band satellite-ground clock observations. We discuss the applications of this algorithm by assessing the clock performance of all BDS3 satellites equipped with a passive hydrogen maser (PHM) or rubidium atomic clock. After investigating the proper prediction model for each satellite, we use the full-ISL algorithm for 24-h clock predictions. The constant hardware delays in the ISL measurements are calibrated by comparing the derived clock parameters with TWSTFT measurements; the full-ISL clock products show high accuracy and continuity. The BDS3 PHMs and rubidium clocks both have a small clock rate drift of 10^{-20} s/s^2. The frequency stability of the BDS3 PHMs and some rubidium clocks is approximately $6–9 \times 10^{-15}$ at 1-day intervals. A linear model is suitable for these small-drift clocks, while a quadratic model is essential for the other rubidium clocks. Applying the full-ISL clock prediction method improves the RMS of the 24 h prediction error from 0.88 to 0.75 ns for PHMs and from 2.62 to 1.64 ns for rubidium clocks. The estimated ISL hardware delay STDs are less than 0.2 ns, and the prediction errors evaluated with TWSTFT clock observations are similar to those evaluated with Ka-band clock observations.

Keywords BDS3 · ISL · TDMA · Allan deviation · Full-ISL clock offset estimation · Clock prediction

Introduction

The third-generation Beidou Navigation Satellite System (BDS3) has been providing basic global navigation services since December 2018 with a constellation of 18 satellites distributed in 3 medium earth orbit (MEO) planes. Additionally, another satellite has been launched into geostationary orbit (GEO), but it is not yet operational. An overview of the BDS3 satellites currently in orbit is shown in Table 1. The complete space segment of the BDS3 system will employ a hybrid constellation comprising 3 satellites in GEO, 3 satellites in inclined geosynchronous orbit (IGSO), and 24 satellites in MEO. To provide a frequency standard for the BDS3 system, the BDS3 satellites are equipped with two types of atomic clocks, namely a passive hydrogen maser (PHM) and a rubidium clock. Two main observational methods are utilized in combination to calculate satellite clock offsets. The L-band two-way satellite time and frequency transfer (TWSTFT) method is used to obtain clock offsets relative to ground stations, using a regional monitoring network. Ka-band inter-satellite link (ISL) measurements are used with a time division multiple access (TDMA) mode to obtain clock offsets relative to other satellites or ground stations.

The TWSTFT method provides high-precision satellite clock measurements and has been used for clock determination and prediction purposes since the second-generation Beidou Navigation Satellite System (BDS2) was operational (Liu et al. 2009; Han et al. 2013; Zhou et al. 2016; Tang

✉ Junyang Pan
panjy@shao.ac.cn

1 Shanghai Astronomical Observatory, Chinese Academy of Sciences, Shanghai 200030, China

2 University of Chinese Academy of Sciences, Beijing 100049, China

3 Shanghai Key Laboratory for Space Positioning and Navigation, Shanghai 200030, China

4 Beijing Satellite Navigation Center, Beijing 100094, China

Table 1 Space segment of the BDS3 satellite constellation (as of April 1, 2019, all satellites are operational except G1 is in checkout status, and the nominal semimajor axis for all MEO satellites in 21, 500 km)

Satellite	Launch date Yyyy-mm-dd	PRN	Nominal clock
M1	2017–11-05	C19	Rb
M2	2017–11-05	C20	Rb
M7	2018–01-11	C27	PHM
M8	2018–01-11	C28	PHM
M3	2018–02-12	C21	Rb
M4	2018–02-12	C22	Rb
M9	2018–03-29	C29	PHM
M10	2018–03-29	C30	PHM
M5	2018–07-29	C23	Rb
M6	2018–07-29	C24	Rb
M11	2018–08-24	C25	PHM
M12	2018–08-24	C26	PHM
M13	2018–09-19	C32	Rb
M14	2018–09-19	C33	Rb
M15	2018–10-15	C34	Rb
M16	2018–10-15	C35	Rb
G1	2018–11-01	C59	PHM
M17	2018–11-18	C36	Rb
M18	2018–11-18	C37	Rb

et al. 2016). Moreover, TWSTFT clock measurements have helped improve the precise orbit determination (Zhou et al. 2011; Zhou et al. 2012) and orbit recovery accuracy with a regional monitoring network after maneuvers (Guo et al. 2015). However, with a regional monitoring network, only a 40% clock tracking coverage can be achieved for MEO satellites by TWSTFT (Zhou et al. 2013). To compare with the other clock offset solutions, the L-band TWSTFT is also called the no-ISL solution.

The ISL technology was first proposed for the autonomous satellite navigation of Global Positioning System (GPS) satellites (Ananda et al. 1990). Today, ISL communication is an important component of modern global navigation satellite systems (GNSSs) (Maine et al. 2003; Holmes and Raghavan, 2004; Avila-Rodriguez et al. 2007). Beginning with the GPS BLOCK IIR series of satellites, an ultrahigh frequency (UHF) and frequency-hopping spread spectrum system was adopted in combination with a TDMA scheme (Rajan 2002, 2003). The first Ka-band ISL experiment was conducted on a new-generation BDS satellite constellation. Ka-band ranging, which has high accuracy and a strong resistance against interference, was proposed to replace UHF ISL on GPS BLOCK III satellites (Maine et al. 2003). In addition to providing autonomous navigation, Ka-band ISL was employed to support the precise orbit determination and time synchronization of new-generation BDS satellites. Accordingly, with support from ISL measurements, satellite laser ranging residuals reached 15.0 cm for IGSO satellites and 10.0 cm for MEO satellites (Tang et al. 2018). Furthermore, the clock tracking coverage was increased by more than 40% for MEO satellites (Pan et al. 2018).

Optical ISL has been proposed for low earth orbit and MEO satellites of Kepler Project in a multihop fashion, thereby enabling the direct synchronization of satellites. Although the system time can be generated by a time scale algorithm using ISL relative clock offsets between satellites, a single monitoring and control station is still necessary to maintain alignment with earth rotation, synchronization with the Universal Time Coordinate (UTC), and the ability to control the system (Günther 2018).

To date, PHMs have been used as a frequency standard for BDS and Galileo navigation signals. A PHM has the advantage of exhibiting low-frequency drift over a long period. In Table 1, a PHM is utilized as the nominal clock for seven BDS3 satellites, while a rubidium clock is used for the other twelve BDS3 satellites. Steigenberger and Montenbruck (2017) analyzed Galileo clock products and showed that the stability of the Galileo PHM frequency could reach 10^{-14} at 10^4 s intervals. Subsequently, Wu et al. (2018) introduced the PHM onboard new-generation BDS experimental satellites and evaluated their in-orbit performance: their frequency stability is approximately 6×10^{-15} at 1-day intervals, and the 15-day clock rate variation of the BDS PHM is -1.83×10^{-14} s/s, which is better than those of the Galileo PHMs.

In this study, we propose a full-ISL clock offset estimation and prediction algorithm and assess the accuracy of the BDS3 time synchronization. Currently, TWSTFT measurements are used to set the clocks, while the satellites are visible to the monitor sites located in China, and ISL measurements are used to estimate the clocks that are outside of the viewing area. This method is called the limited-ISL solution. In our full-ISL algorithm, all satellites are synchronized using Ka-band inter-satellite clock observations, and the constellation is synchronized to the system time in Beidou Time (BDT) using Ka-band satellite-ground clock observations. The idea is similar to Kepler Project (Günther 2018), but the observations are established in the Ka-band. By processing clock estimation or prediction parameters of all satellites simultaneously, the impacts of link-specific measurement noise and remaining modeling errors can be reduced. Therefore, clock offset estimations with high continuity and high accuracy can be obtained. We investigate the onboard clock frequency stability and clock rate drift characteristics using our full-ISL clock offset and clock rate estimation procedure. We further investigate the applicability of polynomial fitting to improve the 24-h clock prediction accuracy and conduct a full-ISL clock prediction using a

suitable model for each satellite. The hardware delay represents a key factor that affects the time synchronization of a constellation. For ISL payloads, each satellite hardware delay and clock offset cannot be decoupled by ISL measurements only. A previous study has proposed a hardware delay estimation method based on a comparison of clock offsets (Pan et al. 2018). Herein, we propose a hardware delay estimation method based on a comparison of clock offset parameters conducted during the full-ISL clock prediction process. TWSTFT clock observations are used both as reference clock offsets for the hardware delay estimation and as validation for the clock prediction accuracy.

We first introduce the current time synchronization method supported by ISL measurement. We then propose our full-ISL clock estimation method and compare the full-ISL clock offsets with the present clock offsets. The onboard clock frequency stability and clock rate drift characteristics using our full-ISL clock offset and clock rate estimation procedure are then investigated. We address a suitable prediction model for each satellite, propose a new hardware delay estimation method and conduct a full-ISL clock prediction process. This is followed by a summary and conclusions.

BDS3 satellite clock offset measurements

The regular time of BDS satellites is synchronized to a ground control station based on the system time in BDT using L-band TWSTFT (Liu et al. 2009; Han et al. 2013; Zhou et al. 2016). The TWSTFT technique is also used to synchronize two ground stations (Hackman et al. 2006; Jiang et al. 2017). The basic principles are described as follows.

Both a satellite S and a station G separately transmit L-band pseudorange signals to each other under the control of their respective local atomic clocks. The satellite clock offset relative to the station is calculated from the difference between the uplink and the downlink pseudorange measurements as,

$$d\tau_{sat} - d\tau_{rcv} = \left[\left(\rho_{up} - r_{up} - \Delta\delta_{up}^{ion}\right)\right] - \left(\rho_{down} - r_{down} - \Delta\delta_{down}^{ion}\right)\Big]/(2 * c) \quad (1)$$

where ρ_{up} and ρ_{down} are the uplink and the downlink pseudorange measurements, r_{up} and r_{down} are the uplink and the downlink geometrical distance, $\Delta\delta_{up}^{ion}$ and $\Delta\delta_{down}^{ion}$ are the uplink and the downlink ionospheric delay, $d\tau_{sat}$ and $d\tau_{rcv}$ are the clock offset of satellite and station, and c is the speed of light.

Additionally, BDS3 satellites conduct Ka-band ISL measurements in TDMA mode. This process corresponds to two visible satellites successively sending measurement signals to accomplish one inter-satellite measurement. These ISL measurements must be transformed into a common epoch using a broadcast ephemeris. The difference between these dual one-way measurements is used for the clock offset estimation:

$$clk_A(T_0) - clk_B(T_0) = \frac{\left(\rho_{BA}(T_0) - r_{BA}\right) - \left(\rho_{AB}(T_0) - r_{AB}\right)}{2 * c} + \frac{\tau_A^{tr} - \tau_A^{rcv}}{2} - \frac{\tau_B^{tr} - \tau_B^{rcv}}{2} + \frac{\Delta\delta_{AB} - \Delta\delta_{BA}}{2 * c} \quad (2)$$

where subscripts A and B represent satellite A and satellite B, respectively. Subscripts AB and BA represent the one-way pseudorange measurement, where the first satellite is the transmitter and the second is the receiver. ρ is the pseudorange measurement. r is the geometrical distance between the transmitter and the receiver. $clk(T_0)$ is the clock offset at epoch T_0, and τ^{tr} and τ^{rcv} are the transmitting hardware delay and receiving hardware delay for a satellite, respectively. c is the speed of light. $\Delta\delta$ are corrections that can be easily modeled for the measurement. For a satellite-to-satellite measurement, these corrections include the satellite phase center offsets and relativistic effect correction, and for a satellite-to-ground measurement they include the satellite phase center offsets, relativistic effect correction, receiver variations, troposphere delay, and tidal effect correction. Each pair of the dual one-way measurements is carried out in 3 s. So most of the corrections, except relativistic effect correction, cancel for the clock offset estimation. However, the length of interval of each link can vary with time due to visibility between satellites and the need for communication. For example, the link sequence of satellite A could be {AB,AC,AB,AD,AE,AB……}, and the epoch intervals of link AB are {6 s,9 s……}.

The theory employed to calculate the relative clock offset between a Ka-band satellite and ground anchor station is the same as that for the inter-satellite case. Since the Ka-band and L-band antennas on the ground are located at the main control station, which keeps the system time in BDT, the clock offsets of the station are not discussed and are considered constant. Since only the relative clock offset between satellite and the system time matters, the constant can be any value. For convenience, we set the clock offsets of the station to 0.

The L-band clock offsets considered in this study are obtained from a regional network within China's borders. The present BDS3 clock determination strategy, as introduced in Pan et al. (2018), can be described as follows. For satellite A, the clock offset $clk_A(t)$ at epoch t is

$$clk_A(t) = clk_A^L(t) \quad (3)$$

or

$$clk_A(t) = clk_B^L(t) + clk_{AB}^{ISL}(t) \tag{4}$$

where $clk_A^L(t)$ and $clk_B^L(t)$ are the L-band TWSTFT clock offset measurement of satellite A and satellite B, respectively. $clk_{BA}^{ISL}(t)$ is the calibrated ISL relative clock offset between satellite A and satellite B. The ISL clock offset measurement of a single satellite is only used when it is outside China's border and only the inter-satellite clock offsets are utilized. The present BDS3 clock determination is a combination of L-band clock offsets and Ka-band clock offsets. We call it the limited-ISL solution. A regular polynomial least-squares fitting of the limited-ISL clock offsets is conducted for the broadcast clock parameters of each satellite, respectively.

Taking satellite C24, for instance, Fig. 1 shows the clock prediction error for the limited-ISL model. The clock prediction error is the difference between the clock offset determined from the measurements and the clock offset calculated from the clock offset parameters. The clock offset measurements are the limited-ISL solutions. As shown in Fig. 1, with support from the ISL measurements of all 18 satellites, the entire clock tracking coverage for the MEO BDS3 satellite is achieved. Thus, broadcast clock parameters can be updated hourly, resulting in stable prediction errors within or outside China's borders. The average satellite clock offset uncertainty over MEO satellites is 1.55 ns (Yang et al. 2020a, b).

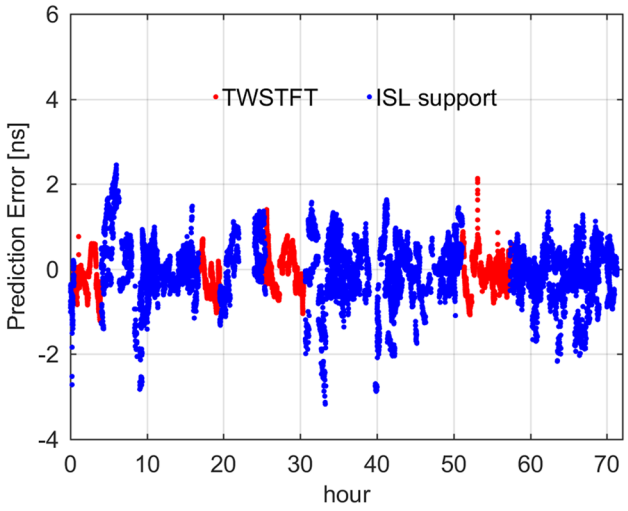

Fig. 1 Prediction Error of BD3 satellite C24 for limited-ISL model

Full-ISL clock estimation

In this section, the full-ISL clock estimation is conducted using ISL measurements from 18 MEO satellites, 1 GEO satellite, and one ground anchor station during the period from February 1 to February 14, 2019. The full-ISL clock offset estimations are compared with other satellite clock offset solutions.

Full-ISL clock algorithm

The uncalibrated ISL relative clock offset measurement $clk_{AB}(t)$ at epoch time t can be expressed in a form of clock offset parameters and hardware delays:

$$\begin{aligned} clk_{AB}(t) = &\left(A_0^A + A_1^A(t-t_0) + A_2^A(t-t_0)^2 - X_{delay}^A\right) \\ &- \left(A_0^B + A_1^B(t-t_0) + A_2^B(t-t_0)^2 - X_{delay}^B\right) + \varepsilon_{AB} \end{aligned} \tag{5}$$

where $X_{delay}^A = \frac{\tau_A^{tr} - \tau_A^{rcv}}{2}, X_{delay}^B = \frac{\tau_B^{tr} - \tau_B^{rcv}}{2}$, ε_{AB} is the measurement noise, A and B are either a satellite or a ground anchor station, and A_0, A_1, and A_2 are the clock offset, clock rate and clock rate drift parameter at reference epoch time t_0, respectively. We assume that the hardware delays of ISL payloads are common constants among different links; constants A_0^A and X_{delay}^A cannot be decoupled from the clock offsets by ISL measurements alone.

Consider a simple clock network consisting of 3 clocks A, B, and C, which are either onboard a satellite or at the anchor station. The relative clock offsets between two satellites or between the ground anchor station and one satellite are obtained by (2). We choose C as the common clock reference, and then the clock parameters of A and B can be estimated simultaneously with a certain arc length of acquired data using least-squares estimation:

$$\mathbf{L} = \mathbf{AX} + \boldsymbol{\varepsilon} \tag{6}$$

$$\mathbf{L} = \begin{bmatrix} clk_{AC}(t_{1,AC}) \\ \vdots \\ clk_{AC}(t_{n_1,AC}) \\ clk_{BC}(t_{1,BC}) \\ \vdots \\ clk_{BC}(t_{n_2,BC}) \\ clk_{AB}(t_{1,AB}) \\ \vdots \\ clk_{AB}(t_{n_3,AB}) \end{bmatrix}_{(n_1+n_2+n_3)\times 1} \tag{7}$$

$$\mathbf{A}=\begin{bmatrix} 1 & (t_{1,AC}-t_0) & 0 & 0 & (t_{1,AC}-t_0)^2 & 0 \\ \vdots & \vdots & \vdots & \vdots & \vdots & \vdots \\ 1 & (t_{n_1,AC}-t_0) & 0 & 0 & (t_{n_1,AC}-t_0)^2 & 0 \\ 0 & 0 & 1 & (t_{1,BC}-t_0) & 0 & (t_{1,BC}-t_0)^2 \\ \vdots & \vdots & \vdots & \vdots & \vdots & \vdots \\ 0 & 0 & 1 & (t_{n_2,BC}-t_0) & 0 & (t_{n_2,BC}-t_0)^2 \\ 1 & (t_{1,AB}-t_0) & -1 & -(t_{1,AB}-t_0) & (t_{1,AB}-t_0)^2 & -(t_{1,AB}-t_0)^2 \\ \vdots & \vdots & \vdots & \vdots & \vdots & \vdots \\ 1 & (t_{n_3,AB}-t_0) & -1 & -(t_{n_3,AB}-t_0) & (t_{n_3,AB}-t_0)^2 & -(t_{n_3,AB}-t_0)^2 \end{bmatrix}_{(n_1+n_2+n_3)\times 6} \tag{8}$$

$$\mathbf{X}=\begin{bmatrix} A_0^a \\ A_1^A \\ A_0^b \\ A_1^B \\ A_2^A \\ A_2^B \end{bmatrix} \tag{9}$$

where **L** is the vector of observations, **A** is the matrix of the coefficients, **X** is the vector of estimated parameters, **ε** is the vector of measurement noises. $A_0^a = A_0^A - X_{delay}^A$, $A_0^b = A_0^B - X_{delay}^B$, the observation epoch time sequence of links AC, BC, and AB is $[t_{1,AC}, \cdots, t_{n_1,AC}]$, $[t_{1,BC}, \cdots, t_{n_2,BC}]$, and $[t_{1,AB}, \cdots, t_{n_3,AB}]$, respectively, and the number of observation of links AC, BC, and AB is n_1, n_2 and n_3, respectively. n_1 and n_2 should be greater than the order of the polynomial parameters, while link AB is redundant. If $n_3 = 0$, then the clock parameter estimations of A and B are independent. If the clock parameter model is linear model, **A** and **X** would be reduced.

For BDS3, the ground anchor station is connected to the system time in BDT; hence, it is chosen as the common clock reference, and the clock offsets are fixed to 0. Additionally, the clock parameter models depend on the arc length of acquired data and the clock characteristics. The full-ISL clock estimation algorithm will be applied to data acquired from different arc lengths for different purposes. The settings of the estimations are listed in Table 2. The number of satellites with linear or quadratic clock model is m_1 and, m_2, respectively, and m is the sum $m = m_1 + m_2$. Due to the uncertainty of the epoch intervals, all data are used during the different settings.

The ISL hardware delay estimation is based on the fact that pair-link measurements of a BDS3 satellite are all conducted by the same phased array antenna. Previous research has shown that by taking the combined hardware delay as a constant, the hardware delays of new-generation satellites can be estimated by a clock offset comparison. Accordingly, the accuracy of the hardware delay solution is within 0.3 ns. We propose a clock parameter comparison solution for ISL hardware delays to eliminate abnormal clock measurement variations with the same assumption.

The ISL hardware delay can be estimated by:

$$\begin{aligned} X_{delay}^A &= A_0^A - A_0^a \\ X_{delay}^B &= A_0^B - A_0^b \end{aligned} \tag{10}$$

where A_0^A and A_0^B are the reference A0 parameters of satellites A and B, respectively, and A_0^a and A_0^b are the full-ISL A0 parameters of satellite A and satellite B, respectively.

Table 2 Settings of full-ISL clock algorithm for different purposes

Observations	Ka-band satellite-to-satellite relative clock offsets; Ka-band satellite-to-ground relative clock offsets		
Clock reference	Anchor station		
Arc length	1 min	1 h	48 h
Estimated parameters of each satellite	A_0,A_1	A_0,A_1	A_0,A_1/A_0,A_1,A_2
Total number of estimated parameters	2 m	2 m	2*($m_1 + m_2$)
Used parameters of each satellite	A_0	A_1	A_0,A_1/A_0,A_1,A_2
Purpose	Clock offsets estimation; clock frequency stability analysis	Clock rate variations analysis	Clock prediction; ISL hardware delay estimations

Because the ISL links provide only timing difference data, there is a rank deficiency in their use. This can be resolved if all a referenced to one satellite whose time has been fixed via TWSTFT measurements to a ground station. For a satellite whose polynomial offsets were determined by ISL links, this can take the form of fitting its A0 term of a 48-h full-ISL solution to TWSTFT measurements. Redundant observations could be made by fitting to the A0 terms of many satellites, although we have not attempted this.

The differences between full-ISL clock estimation and the algorithm proposed by Pan et al. (2018), i.e., the limited-ISL solution, are listed as follows:

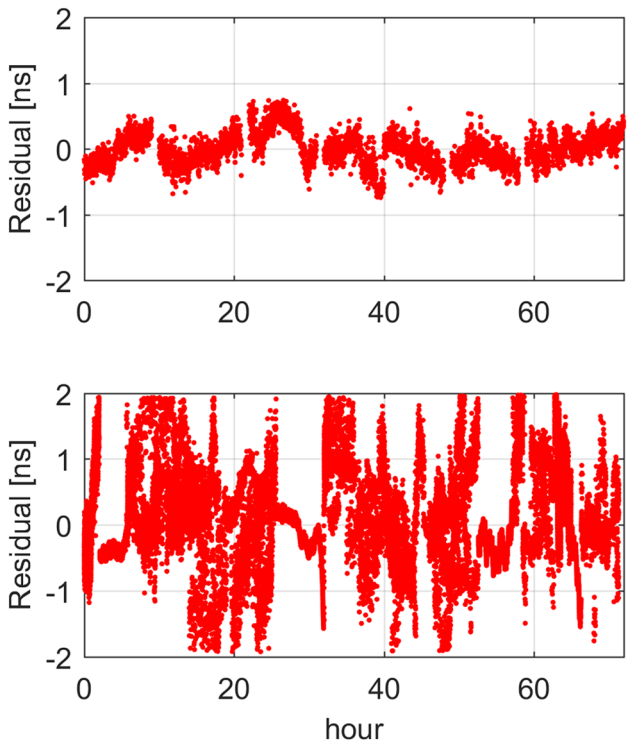

Fig. 2 Clock offset residuals for the full-ISL clock offsets (top) and the limited-ISL clock offsets (bottom) of satellite C25

(1) The limited-ISL solution uses a combination of L-band satellite-to-ground clock measurements with Ka-band satellite-to-satellite measurements when no ground measurements are available, while the full-ISL solution uses Ka-band satellite-to-ground clock offsets and all Ka-band satellite-to-satellite measurements.
(2) Because of (1), the hardware delays of all ISL payloads must be calibrated, in agreement with the downlink L-band navigation signals and broadcast clock offset parameters, before the limited-ISL solution is conducted. This ensures that the L-band and Ka-band could be consistent, while all the estimated hardware delays should be calibrated after the full-ISL solution to quantify their possible variations and limit their effects since only Ka-band measurements are used.
(3) The clock offset parameters of each satellite of the limited-ISL solution are estimated separately using the combined clock offset data, while clock offset parameters of all satellites of full-ISL solution are estimated simultaneously using the ISL clock offset data.

Satellite clock measurements

We first apply the full-ISL clock estimation algorithm to 1-min data consisting of ISL clock observations. The clock parameter models of all satellites are linear. The parameter sequences of A0 are used for 60-s-interval full-ISL clock offset estimations, i.e., the full-ISL clock products.

Figure 2 shows the 3-day arc residuals of the full-ISL and limited-ISL clock offsets of satellite C25. A quadratic curve detrends the full-ISL and limited-ISL clock offsets, and the RMS values of all satellites are listed in Table 3. As shown in the figure, the entire clock tracking coverage for all 18 of the MEO BDS3 satellites can also be achieved by Ka-band full-ISL clock offsets. As shown in the table, the fitting accuracy of the full-ISL clock offsets is approximately 0.3 ns (root mean square, RMS), while the fitting accuracy of the limited-ISL clock offsets reaches approximately 0.6 ns (RMS). Those times when there are much lower residuals

Table 3 Fitting accuracy of the full-ISL and limited-ISL clock offsets (RMS, unit: ns)

PRN	Manufacturer	Full-ISL	Limited-ISL	PRN	manufacturer	Full-ISL	Limited-ISL
C19	CASC	0.27	0.71	C29	SECM	0.22	0.59
C20	CASC	0.25	0.68	C30	SECM	0.25	0.41
C21	CASC	0.37	0.82	C32	CASC	0.22	0.52
C22	CASC	0.26	0.64	C33	CASC	0.29	0.77
C23	CASC	0.32	0.63	C34	SECM	0.23	0.94
C24	CASC	0.34	0.51	C35	SECM	0.22	0.82
C25	SECM	0.25	0.62	C36	CASC	0.21	0.50
C26	SECM	0.28	0.96	C37	CASC	0.25	0.36
C27	SECM	0.22	0.60	C59	CASC	0.31	0.30
C28	SECM	0.23	0.64	Mean		0.26	0.63

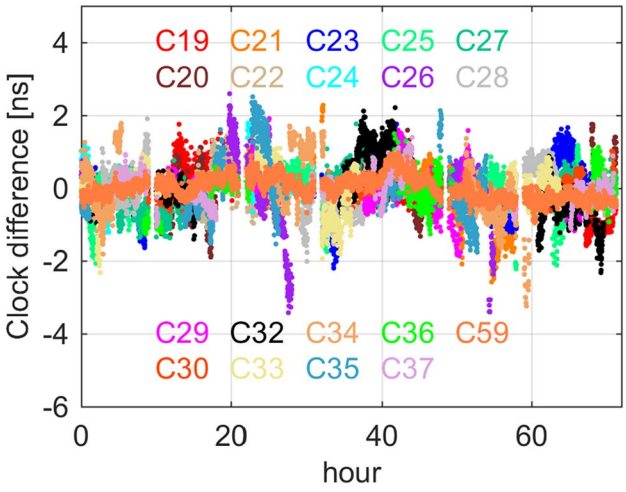

Fig. 3 Time series of the full-ISL and no-ISL clock differences of the BDS3 satellites

Table 4 Full-ISL and no-ISL clock differences: mean and STD (unit: ns)

PRN	Mean	STD	PRN	Mean	STD
C19	2614.001	0.70	C29	1594.487	0.59
C20	2612.048	0.58	C30	1603.730	0.26
C21	2613.089	0.93	C32	37,843.614	0.78
C22	2613.040	0.43	C33	2619.156	0.67
C23	36,556.553	0.65	C34	1594.650	0.85
C24	2614.582	0.42	C35	1593.420	0.89
C25	1642.975	0.61	C36	37,845.568	0.50
C26	1641.146	1.01	C37	2617.413	0.42
C27	1665.139	0.58	C59	2847.872	0.30
C28	2270.259	0.60			

are the TWSTFT clock data since the ISL support part may contain observation anomalies of multiple satellites' TWSTFT clock data. The full-ISL clock offsets appear to represent the better option with regard to both continuity and accuracy.

Figure 3 shows the differences in the full-ISL and no-ISL 3-day arc clock data. Considering the constant differences between the two datasets, the mean is eliminated from the clock difference time series in the figure. Table 4 shows the mean values and standard deviations (STDs) of the differences between full-ISL and no-ISL clock. The time series show obvious variations, which may be related to the residual ionospheric delays between the uplink and downlink pseudorange since the frequencies of the uplink and downlink signals are different. Table 4 shows that the Ka-band measurements still suffer from a severe constant error. Some clustering of the offset values can be seen, e.g., {C19,C20,C21,C22, C24, C27, C33} which is expected since the Ka-band signal transmitting equipment and receiving equipment of these satellites are from the same manufacturer.

Characteristics of onboard atomic clocks

There are two types of atomic clocks onboard the BDS3 satellites: the PHM and rubidium clock, which have different frequency accuracy and frequency rate drift characteristics. The onboard atomic clock performance plays a significant role in satellite navigation system services and is often measured by the Allan deviation (Allan 1987; Zhou et al. 2016). The onboard atomic clock rate variation constitutes a crucial factor that restricts the long-term autonomous time-keeping capability of the satellite clock (Wu et al. 2018). Therefore, we investigate the Allan deviations and clock rate characteristics of the satellite clocks to assess their performance.

Clock rate variations

We compare the clock rate drifts of different BDS3 satellite clocks. For this purpose, the full-ISL clock algorithm uses 1-h Ka-band inter-satellite and satellite-ground clock observations to fit the satellite clock rates. In data with a length of 1 h, the rate drifts of rubidium and PHM clocks are negligible, so a linear fitting scheme is suitable, but only the A1 parameter estimations of each satellite are used as the time sequence of the clock rate. For comparison, we set all satellite clock rates to zero at the start time epoch.

Figure 4 shows the linear fitting residuals of the consecutive 720-h clock rate sequences of some satellites. Table 5 shows the clock rate drifts and fitting RMSs of all satellites. As shown in the figure and table, the clock rate residual sequences are nearly white noise, and the fitting RMSs are at 10^{-14} s/s level, except for that of satellite C19, whose curve displays a clock frequency drift variation and the fitting RMS reaches 10^{-13} s/s level. The clock rate drifts of all BDS3 PHMs are 10^{-20} s/s^2, ranging from -1.54×10^{-20} to -4.46×10^{-20} s/s^2, which are similar to those of the Galileo PHMs (Wu et al. 2018). The clock rate drifts of the BDS3 rubidium clocks are mainly 10^{-18} to 10^{-19} s/s^2, except for satellite C34, whose clock rate drift is 5.59×10^{-20} s/s^2. Since the variation in the clock frequency drift of C19 will affect the clock offset modeling and prediction results, satellite C19 is excluded from our discussion. In real conditions, due to the entire clock tracking coverage, the clock offset parameters can be updated hourly. The impact of the clock

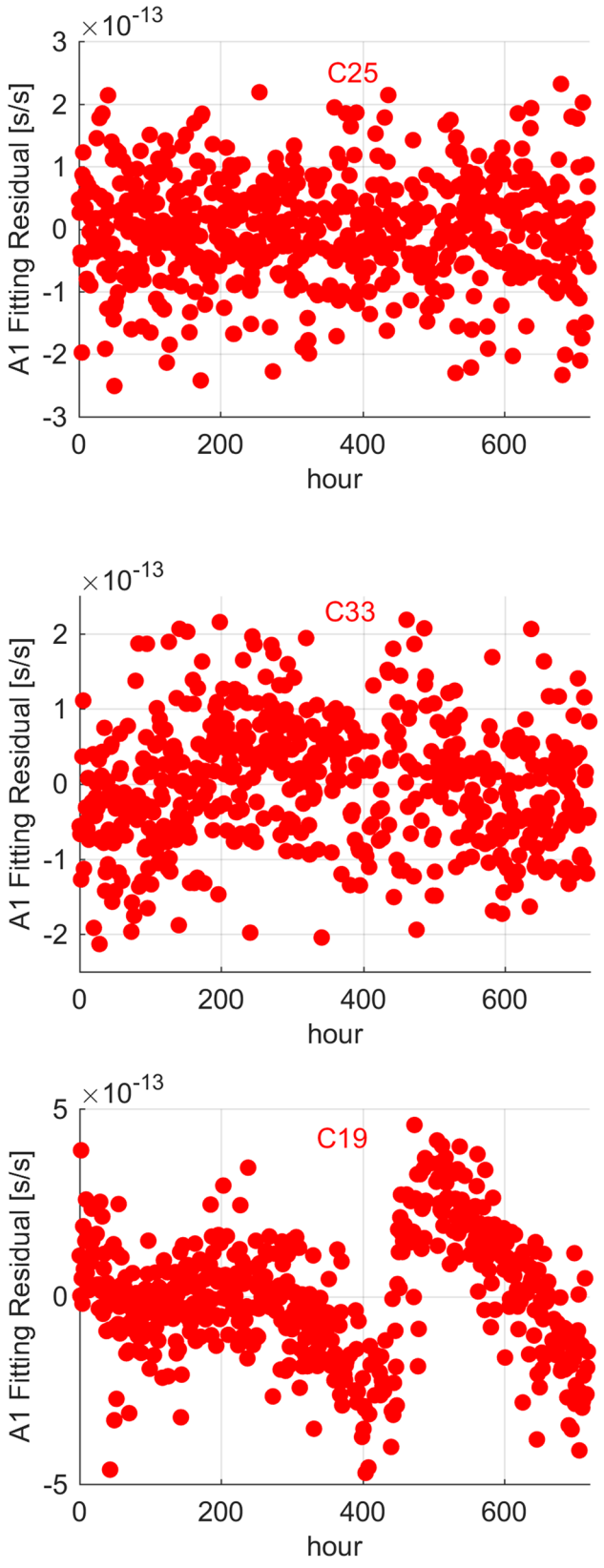

Fig. 4 Clock rate fitting residuals of a PHM (top), a rubidium clock (middle) of BDS3 satellite, and of BDS3 satellite C19 (bottom)

frequency drift variation on the accuracy of broadcast clock offset parameters can be negligible.

Clock frequency stability

The frequency stability of BDS3 satellite clocks is analyzed. The improved estimation method for the Allan variance described by Sesia (2008) is used to reduce the influence of missing data on the analysis.

The Allan deviation (ADEV) values calculated from the 15-day arc of full-ISL BDS3 satellite clock products are shown in Fig. 5 and Table 6. We evaluate only the long-term stability of the satellite clocks due to the large noise level of Ka-band measurements and their impact on short-term ADEV estimations (Wu et al. 2018). The frequency drift of each satellite clock is removed to calculate the long-term ADEV. The stability of BDS3 satellite clocks is approximately 4×10^{-14} at the 10^4 s interval for both the PHMs and the rubidium clocks. The ADEV of clocks onboard the new generation BDS experimental MEOs has shown a considerable increase after the 10^4 s interval due to a serious lack of data (Wu et al. 2018). No obvious increase is observed in the ADEV values after the 10^4 s interval. The estimated stability is in agreement with the expected value due to the continuity of the full-ISL clock products. The influence of Ka-band measurement noise on BDS3 ADEV values is approximately 2×10^{-15} at the 86,400-s interval. The stability of the BDS3 PHMs is approximately 7 to 9×10^{-15} at the 86,400-s interval. Some BDS3 rubidium clocks, including those of satellites C19, C24, C32, C36, and C37, show a stability at the 86,400 s interval of approximately $6\sim9\times10^{-15}$, which is the same or even better than those of the BDS3 PHMs. These clocks show a higher frequency stability than the clocks of GPS BLOCK IIF and Galileo satellites (Wu et al. 2018). The stability of the other BDS3 rubidium clocks is approximately 1×10^{-14} at the 86,400-s interval.

Full-ISL clock prediction

In this section, the full-ISL clock prediction is conducted using ISL measurements from 17 MEO satellites, 1 GEO satellite, and one ground anchor station during the period from February 1 to February 14, 2019. The clock offset modeling process may be affected by the clock characteristics. Therefore, we model the clock offset for each satellite. The L-band no-ISL clock measurements acquired during the same period are utilized to estimate the onboard ISL payload hardware delays. Then, the full-ISL clock predictions are compared with Ka-band satellite-ground clock measurements to evaluate the accuracies of the full-ISL clock parameters.

Table 5 Clock rate drifts fitting

Satellite	Nominal clock	Clock rate drift (s/s^2)	Fitting RMS (s/s)	Satellite	Nominal clock	Clock rate drift (s/s^2)	Fitting RMS (s/s)
C25	PHM	− 4.46E−20	7.64E− 14	C22	Rb	−2.00E−18	8.54E−14
C26	PHM	− 2.33E−20	8.53E− 14	C23	Rb	−3.07E−18	7.02E−14
C27	PHM	− 2.81E−20	7.93E− 14	C24	Rb	−3.31E−18	7.38E−14
C28	PHM	− 3.21E−20	9.27E− 14	C32	Rb	−3.15E−18	7.25E−14
C29	PHM	− 1.54E−20	8.02E− 14	C33	Rb	−9.08E−19	9.07E−14
C30	PHM	− 4.19E−20	7.91E− 14	C34	Rb	5.59E−20	7.65E−14
C59	PHM	− 2.52E− 20	4.14E− 14	C35	Rb	−5.41E−19	8.14E−14
C19	Rb	8.95E−17	1.83E− 13	C36	Rb	−1.86E−18	8.89E−14
C20	Rb	− 2.27E−18	8.15E− 14	C37	Rb	−2.55E−18	7.49E−14
C21	Rb	− 1.74E−18	8.03E-14				

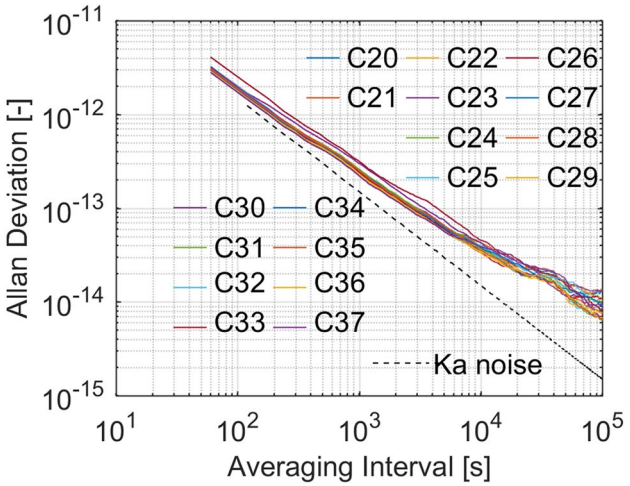

Fig. 5 Allan deviations of the BDS3 satellite clocks evaluated by full-ISL clock products

Clock prediction strategy

The full-ISL clock prediction algorithm is conducted on a 2-day arc of Ka-band inter-satellite and satellite-ground clock observations. The estimated parameter A0 represents a combination of the ISL hardware delay and clock offset of each satellite. Tang et al. (2018) and Pan et al. (2018) showed that the ISL hardware delays mainly affect the A0 parameters. The ground anchor station is connected to the system time in BDT. With the clock offsets of the anchor station fixed at 0, the estimated parameters A1 and A2 of each satellite can be directly utilized as broadcast clock parameters A1 and A2. The clock parameter model is either linear or quadratic; for a linear model, the parameter A2 is fixed at 0. The applicability of polynomial fitting for each satellite is investigated in the following section.

As indicated in (2), relative clock offsets contain the constant hardware delay of satellite A (X^A_{delay}), and the constant hardware delay of satellite B (X^B_{delay}). Since the hardware delay cannot be decoupled from the clock offset by Ka-band measurements alone, L-band no-ISL clock observations are introduced to estimate the ISL hardware delay.

The ISL measurements are processed to conduct full-ISL clock predictions and hardware delay estimations performed every hour to match the broadcast clock offset parameter update cycle. The accuracy of the full-ISL clock prediction is evaluated in terms of fitting residuals and prediction errors.

Table 6 Frequency stability of BDS3 satellite clocks. All values relative to exponent -14

PRN	Nominal clock	10^4-s interval	86,400-s interval	PRN	Nominal clock	10^4-s interval	86,400-s interval
C25	PHM	3.740	0.860	C22	Rb	3.460	1.170
C26	PHM	4.530	0.928	C23	Rb	3.840	1.320
C27	PHM	3.720	0.728	C24	Rb	3.900	0.995
C28	PHM	4.250	0.830	C32	Rb	3.690	0.702
C29	PHM	3.660	0.725	C33	Rb	4.000	1.030
C30	PHM	4.270	0.766	C34	Rb	3.340	1.110
C59	PHM	3.880	0.924	C35	Rb	3.800	1.050
C20	Rb	3.700	1.190	C36	Rb	3.570	0.694
C21	Rb	3.840	1.280	C37	Rb	3.330	0.778

Table 7 Clock offset model comparison (unit: ns)

Satellite	Nominal clock	Clock rate drift(unit: s/s^2)	Linear model		Quadratic model	
			Fitting error (RMS)	24-h prediction error (RMS)	Fitting error (RMS)	24-h prediction error (RMS)
C25	PHM	− 4.46E−20	0.15	1.19	0.13	1.70
C26	PHM	− 2.33E−20	0.17	1.04	0.12	2.76
C27	PHM	− 2.81E−20	0.14	1.43	0.12	3.38
C28	PHM	− 3.21E−20	0.15	0.92	0.14	3.46
C29	PHM	− 1.54E−20	0.14	0.28	0.12	1.34
C30	PHM	− 4.19E−20	0.15	0.51	0.12	1.85
C59	PHM	− 2.52E−20	0.36	0.81	0.30	2.18
C20	Rb	− 2.27E−18	0.78	22.52	0.12	3.10
C21	Rb	− 1.74E−18	0.55	17.29	0.13	2.31
C22	Rb	− 2.00E−18	0.67	20.49	0.12	2.73
C23	Rb	− 3.07E−18	0.66	30.20	0.19	3.33
C24	Rb	− 3.31E−18	0.65	30.04	0.12	2.09
C32	Rb	− 3.15E−18	0.66	30.80	0.14	1.66
C33	Rb	− 9.08E−19	0.28	9.34	0.12	2.33
C34	Rb	5.59E−20	0.15	1.88	0.14	2.69
C35	Rb	− 5.41E−19	0.16	3.96	0.13	3.71
C36	Rb	− 1.86E−18	0.41	19.01	0.11	3.27
C37	Rb	− 2.55E−18	0.84	24.87	0.11	2.38
Mean PHM value	− 3.01E−20	0.18	0.88	0.15	2.38	
Mean Rb value	− 1.94E−18	0.53	19.10	0.13	2.69	

Clock offset modeling

We investigate the proper clock fitting and prediction model for each BDS3 satellite. Usually, satellite clock offsets can be expressed as a polynomial model, either linear or quadratic, according to the length of the data and the clock characteristics. For this purpose, the 48-h Ka-band satellite-ground clock data are adopted to estimate linear and quadratic parameters, and the clock models are applied to both the identical data set and the next 24 h. All the 24-h prediction errors we mentioned refer to the RMS values of the 24-th hour prediction errors.

As shown in Table 7, for all the PHMs and the small-frequency-drift rubidium clocks, the fitting errors of the linear and quadratic models are similar, but the 24-h prediction error of the linear model is smaller than that of the quadratic model. A quadratic model shows better applicability for the other rubidium clocks in terms of both fitting and prediction errors. With the application of the proper clock model, the 24-h prediction accuracies of the PHMs are higher than those of the rubidium clocks.

Table 8 Fitting accuracy of the full-ISL clock estimation (RMS, unit: ns)

Satellite	Polynomial model	Anchor	ISL	Satellite	Polynomial model	Anchor	ISL
C25	Linear	0.20	0.33	C22	Quadratic	0.64	0.37
C26	Linear	0.18	0.34	C23	Quadratic	0.30	0.33
C27	Linear	0.20	0.26	C24	Quadratic	0.17	0.24
C28	Linear	0.23	0.23	C32	Quadratic	0.22	0.27
C29	Linear	0.16	0.24	C33	Quadratic	0.12	0.26
C30	Linear	0.22	0.27	C34	Linear	0.33	0.28
C59	Linear	0.36	0.36	C35	Quadratic	0.23	0.28
C20	Quadratic	0.21	0.26	C36	Quadratic	0.30	0.28
C21	Quadratic	0.33	0.28	C37	Quadratic	0.15	0.26

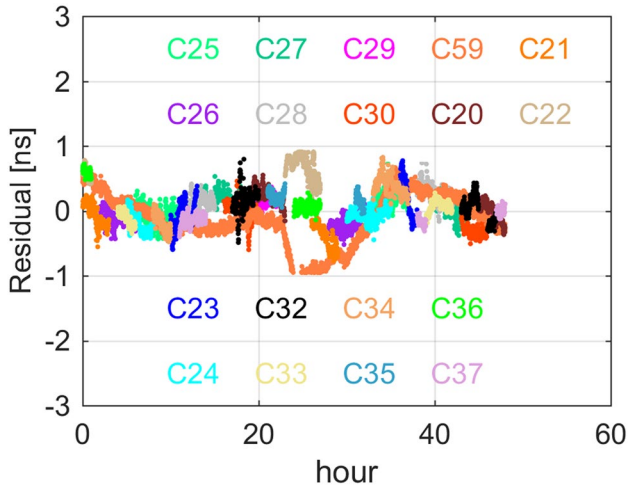

Fig. 6 Anchor clock fitting residuals of the full-ISL clock estimation

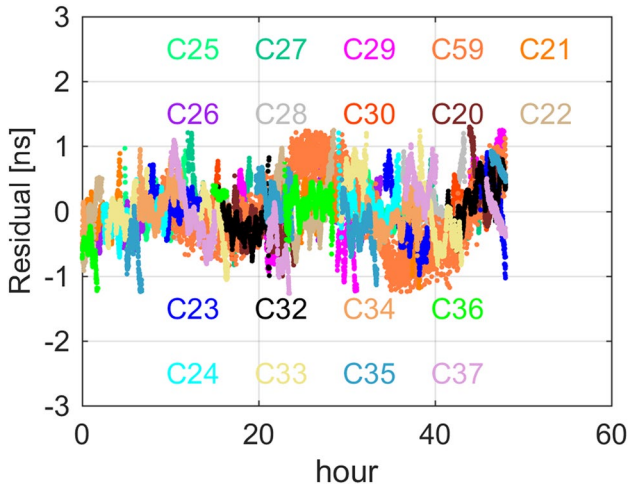

Fig. 7 L-band clock measurement fitting errors

Fitting residuals

Fitting residuals can be used to validate the clock accuracy internally. The measurement noise (the noise of the one-way pseudorange measurements) and clock noise (the physical noise inherent to atomic clock) remain mainly within the fitting residuals. In addition, the fitting residuals may also contain any remaining modeling errors.

The RMS values of the Ka-band satellite-to-satellite clock measurements (ISL clock measurements) and satellite-to-ground clock measurements (anchor clock measurements) are listed in Table 8, and the residuals of the anchor clock measurements are illustrated in Fig. 6. The RMS value of an ISL clock measurement represents the mean RMS value of all satellite-to-satellite links related to each satellite. The fitting accuracy of all ISL clock measurements and anchor clock measurements is approximately 0.3 ns, and the residuals of the ISL clock measurements are identical to those of the anchor clock measurements.

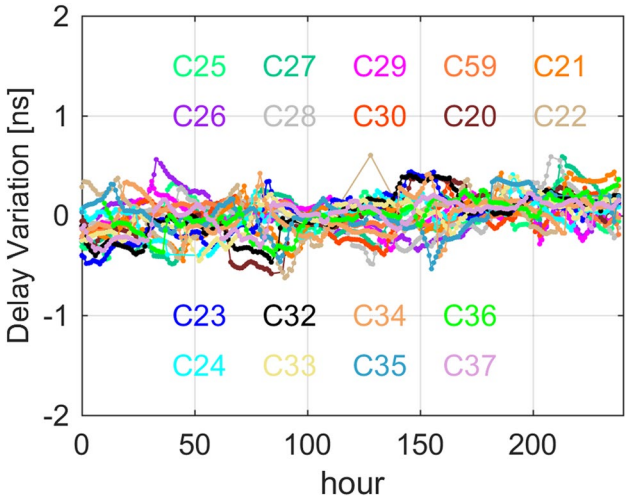

Fig. 8 ISL hardware delay variations for 18 BDS3 satellites

Table 9 ISL hardware delay estimations from full-ISL solution (unit: ns)

Satellite	STD	Satellite	STD
C25	0.15	C22	0.23
C26	0.18	C23	0.21
C27	0.22	C24	0.15
C28	0.20	C32	0.22
C29	0.12	C33	0.16
C30	0.14	C34	0.16
C59	0.09	C35	0.18
C20	0.23	C36	0.17
C21	0.21	C37	0.15
Mean value	0.18		

Hardware delay estimations

The fitting residuals of the no-ISL clock measurements from the 18 BDS3 satellites are shown in Fig. 7. As shown in the figure, no trend is observed for the L-band fitting residual time series, confirming that the A1 and A2 parameters of the full-ISL solution are accurate. Comparing the Ka-band and L-band satellite, a larger and more rapid variation can be observed in the L-band clock offsets. The accuracy of L-band no-ISL clock measurements is approximately 0.4 ns.

The time series of the ISL hardware delay estimations for the 18 BDS3 satellites determined after subtracting the average values of the individual time series are shown in Fig. 8. The STDs of the series are listed in Table 9. As shown in the figure, the ISL hardware delay estimations vary near the

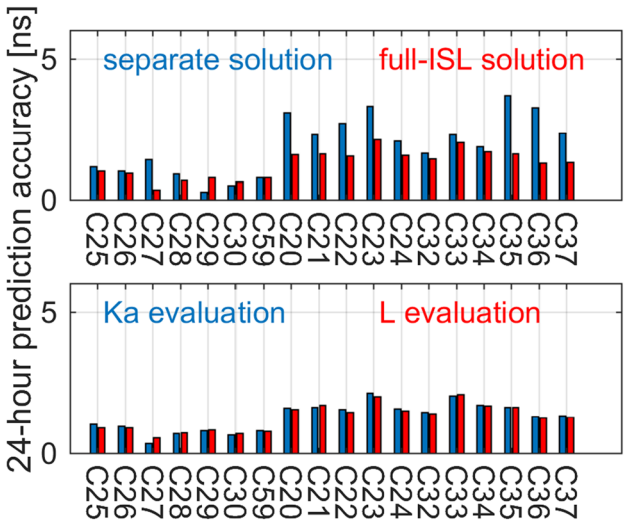

Fig. 9 Comparison of the 24-h clock prediction accuracy between the separate solutions and full-ISL solutions (top) and Ka-band evaluation and L-band evaluation (bottom)

Table 10 24-h clock prediction accuracy of the full-ISL solution (RMS, unit: ns)

Satellite	Ka-band evaluation	L-band evaluation	Satellite	Ka-band evaluation	L-band evaluation
C25	1.02	0.90	C22	1.55	1.47
C26	0.96	0.89	C23	2.14	2.02
C27	0.34	0.54	C24	1.58	1.51
C28	0.71	0.73	C32	1.46	1.40
C29	0.81	0.83	C33	2.04	2.10
C30	0.65	0.69	C34	1.72	1.69
C59	0.79	0.77	C35	1.63	1.64
C20	1.61	1.57	C36	1.30	1.26
C21	1.64	1.72	C37	1.34	1.27
Mean value for PHMs	0.75	0.76	Mean value for rubidium clocks	1.64	1.61

average values, and no trend can be found for the hardware delay series. As the table shows, the STDs of the ISL delay time series for the 18 BDS3 satellites are within 0.2 ns, indicating the high stability of the BDS3 onboard ISL hardware delays. With the hardware delay possessing high stability and Ka-band clock measurements having a high continuity, we suggest our broadcast clock parameter update strategy as following. The clock offset parameters of all satellites are obtained simultaneously by a full-ISL solution, after which the A0 parameter of each satellite is calibrated to broadcast the transmitting signal before being uploaded to the satellite with the hardware delay.

Clock prediction accuracy

The satellite clock prediction accuracy is a crucial factor that directly affects the precision of navigation satellite signals in space. The 24-th hour prediction errors of the full-ISL solutions are evaluated by satellite-ground clock measurements obtained from Ka-band and L-band ranging. The clock prediction accuracy is shown in Fig. 9, and the RMS values are listed in Table 10.

In the top of Fig. 9, the full-ISL solutions are compared with the separate Ka-band solutions and evaluated with Ka-band satellite-ground clock measurements. The Ka-band solutions refer to the separate polynomial fitting of the Ka-band satellite-ground clock measurements for each satellite. By applying the full-ISL solutions, the 24-h clock prediction errors of most satellites are decreased, except for those of satellites C27 and C28, whose errors increased by 0.2 ns but still boast a high accuracy. Moreover, the 24-h clock prediction accuracies are improved from 0.88 to 0.75 ns for PHMs and from 2.62 to 1.64 ns for rubidium clocks. Greater improvements are achieved for the rubidium clocks, while higher accuracies are achieved for the PHMs.

In the bottom of Fig. 9, the full-ISL solutions are evaluated with Ka-band and L-band satellite-ground clock measurements. The prediction accuracies of the Ka-band evaluation are highly consistent with those of the L-band evaluation. This result also validates the hardware delay estimations.

Summary and conclusions

We introduced a time synchronization approach based on L-band TWSTFT and Ka-band TDMA for BDS3 satellites. Then, we proposed a full-ISL clock algorithm based mainly on Ka-band TDMA. We discussed the applications of the full-ISL clock algorithm with regard to assessing the performance of satellite clocks, estimating hardware delays and predicting clock offsets. The conclusions are as follows:

(1) Entire clock tracking coverage can be established by using Ka-band full-ISL clock products. By applying the full-ISL clock algorithm, the clock observation anomalies of each single link can be eliminated. The fitting accuracy of 3-day arc full-ISL clock products is less than 0.3 ns (RMS).
(2) In terms of 24-h prediction, the linear fitting should be applied for all the BDS3 PHMs and all small-frequency drift rubidium clocks, whereas quadratic fitting should be applied for other rubidium clocks.
(3) By applying the full-ISL clock algorithm, the 24-h clock prediction accuracies were improved from 0.88 to

0.75 ns for the PHMs (RMS) and from 2.62 to 1.64 ns for the rubidium clocks (RMS). Greater improvements were achieved for rubidium clocks, while higher accuracies were achieved for PHMs. ISL hardware delays were estimated using a clock parameter comparison method, and the STDs were within 0.2 ns for the 18 BDS3 satellites. Similar clock prediction and hardware delay estimation accuracies can be achieved with only one GEO satellite connected to the reference time in BDT.

The above results indicate that we can obtain clock products and parameters that boast high continuity, high accuracy, and high stability with a full-ISL clock algorithm using Ka-band ISL and satellite-ground clock measurements.

Acknowledgements This work was supported by ZFS (Y9E0151M26), the National Key Research Program of China as the "Collaborative Precision Positioning Project" (No. 2016YFB0501900), the National Natural Science Foundation of China (Grant Nos. 41574029, 61603397), and the Youth Innovation Promotion Association of the Chinese Academy of Sciences (CAS) (Grant No. 2016242).

Data Availability The BDS3 ISL measurements and TWSTFT data are available from the corresponding author upon request.

References

Allan DW (1987) Time and frequency (Time-Domain) characterization, estimation, and prediction of precision clocks and oscillators. IEEE Trans Ultrason Ferroelectr Control (UFFC) 34(6):647–654

Ananda M, Bernstein H, Cunningham K, Feess W, Stroud E (1990) Global positioning system (GPS) autonomous navigation. IEEE Symposium on Position Location and Navigation Symposium A Decade of Excellence in the Navigation Sciences. IEEE March 20, https://doi.org/10.1109/PLANS.1990.66220

Avila-Rodriguez J, Wallner S, Hein G, Eissfeller B (2007) A vision on new frequencies, signals and concepts for future GNSS systems. Proc. ION GNSS 2007, Institute of Navigation, Fort Worth, TX, September 25–28, 517–534.

Günther C (2018) Kepler - satellite navigation without clocks and ground infrastructure. Proc. ION GNSS+ 2018, Institute of Navigation, Miami, Florida, September 2018, 849–856. https://doi.org/10.33012/2018.15997

Guo R, Zhou J, Hu X et al (2015) Precise orbit determination and rapid orbit recovery supported by time synchronization. Adv Space Res 55(12):2889–2898

Hackman C, Levine J, Parker TE (2006) A Long-Term Comparison of GPS Carrier-phase Frequency Transfer and Two-Way Satellite Time/Frequency Transfer. Proceedings of the 38th Annual Precise Time and Time Interval Systems and Applications Meeting, Institute of Navigation, Reston, Virginia, USA, December 7–9, 485–498.

Han S, Gui Q, Li J (2013) Establishment criteria, routing algorithms and probability of use of inter-satellite links in mixed navigation constellations. Adv Space Res 51(11):2084–2092

Holmes J, Raghavan S (2004) A summary of the new GPS IIR-M and IIF modernization signals. IEEE Vehicular Technology Conference, September 26–29, https://doi.org/10.1109/VETECF.2004.1404854

Jiang Z, Z V, Parker, TE, Yao J, Huang, Y, Lin S (2017) Accurate TWSTFT Time Transfer with Indirect Links. Proc. ION PTTI 2017, Institute of Navigation, Monterey, California, USA, January 30–2, 243–255.

Liu L, Zhu L, Han C, Liu X, Li C (2009) The model of radio two-way time comparison between satellite and station and experimental analysis. Chin Astron Astrophy 33(4):431–439

Maine K, Anderson P, Langer J (2003) Crosslinks for the next-generation GPS. IEEE Aerospace Conference, March 8–15, https://doi.org/10.1109/AERO.2003.1235087

Pan J, Hu X, Zhou S, Tang C, Guo R, Zhu L, Tang G, Hu G (2018) Time synchronization of new-generation BDS satellites using inter-satellite link measurements. Adv Space Res 61(1):145–153

Rajan J (2002) Highlights of GPS II-R Autonomous Navigation. The 58th Annual Meeting of The Institute of Navigation and CIGTF 21st Guidance Test Symposium (2002), Albuquerque, NM, June 2002, 354–363.

Rajan J, Orr M, Wang P (2003) On-Orbit Validation of GPS IIR Autonomous Navigation. The 59th Annual Meeting of The Institute of Navigation and CIGTF 22nd Guidance Test Symposium (2003), Albuquerque, NM, June 2003, 411–419

Steigenberger P, Montenbruck O (2017) Galileo status: orbits, clocks, and positioning. GPS Solut 21(2):319–331. https://doi.org/10.1007/s10291-016-0566-5

Sesia I (2008) Estimating the Allan variance in the presence of long periods of missing data and outliers. Metrologia 45(6):134–142

Tang C et al (2016) Improvement of Orbit Determination Accuracy for Beidou Navigation Satellite System with Two-Way Satellite Time Frequency Transfer. Adv Space Res 58(7):1390–1400

Tang C et al (2018) Initial results of centralized autonomous orbit determination of the new-generation BDS satellites with inter-satellite link measurements. J Geodesy 92(10):1155–1169

Wu Z, Zhou S, Hu X, Liu L, Shuai T, Xie Y, Tang C, Pan J, Zhu L, Chang Z (2018) Performance of the BDS3 experimental satellite passive hydrogen maser. GPS Solut 22:43. https://doi.org/10.1007/s10291-018-0706-1

Yang Y, Mao Y, Sun B (2020a) Basic performance and future developments of BeiDou global navigation satellite system. Satellite Navigation 1(1):1–8

Yang Y, Yang Y, Hu X, Chen J, Guo R, Tang C, Zhou S, Zhao L, Xu J (2020b) Inter-Satellite Link Enhanced Orbit Determination for BeiDou-3. J Navig 73(1):115–130

Zhou S et al (2011) Orbit determination and time synchronization for a GEO/IGSO satellite navigation constellation with regional tracking network. Sci China Phys Mech Astron 54:1089–1097

Zhou S, Cao Y, Zhou J, Hu X, Tang C, Liu L, Guo R, He F, Chen J, Wu B (2012) Positioning accuracy assessment for the 4GEO/5IGSO/2MEO constellation of COMPASS. Sci China Phys Mech Astron 55:2290–2299

Zhou S et al (2013) Accuracy analyses of precise orbit determination and timing for COMPASS/Beidou-2 4GEO/5IGSO/4MEO constellation. Lecture Notes Electrical Eng 245:89–102

Zhou S, Hu X, Liu L, Guo R, Zhu L, Chang Z, Tang C, Gong X, Li R, Yu Y (2016) Application of two-way satellite time and frequency transfer in the Beidou navigation satellite system. Sci China Phys Mech Astron 59:109511

Junyang Pan received his bachelor's degree from Nanjing University in 2014, and is a Ph.D. student at Shanghai Astronomy Observatory, China Academy of Sciences. His research focuses on time synchronization of navigation satellites and precise GNSS data processing.

Xiaogong Hu received his Ph.D. degree from Shanghai Astronomy Observatory in 1999, where he is an associate director at the Center for Astro-geodynamics Research. His research focuses on orbital mechanics of aircraft and applications in satellite navigation and deep space exploration. His current research interests are signal in space service performance of GPS, Galileo, and BDS navigation system.

Shanshi Zhou received her master's degree from Tongji University in 2007, and Ph.D. degree from Shanghai Astronomy Observatory in 2011. She is an associate research fellow at Shanghai Astronomy Observatory, China Academy of Sciences. Her current research interests are GNSS satellite orbit determination and time synchronization and satellite atomic clock behavior monitoring and evaluation.

Chengpan Tang received his bachelor's degree from Central South University in 2011 and Ph.D. degree from Shanghai Astronomy Observatory in 2017. He is an assistant research fellow at Shanghai Astronomy Observatory, China Academy of Sciences. His research focuses on precise orbit determination of navigation satellites and precise GNSS data processing.

Dongxia Wang received her Ph.D. degree from Beihang University in 2013, and is an engineer in the Department of operational control at Beijing Satellite Navigation Center, China. Her current research focuses on Time Synchronization and Inter-satellite Link technology.

Yufei Yang received his master's degree from Information Engineering University in 2013, and is currently a Ph.D. student at Information Engineering University. He is an engineer at Beijing Satellite Navigation Center. His current research interests are navigation satellite orbit and clock estimation using inter-satellite link.

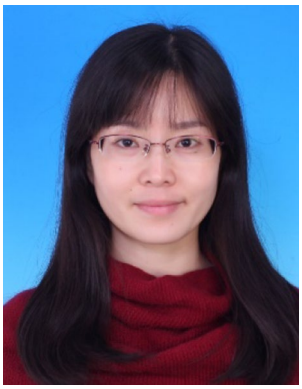

Wenli Dong received her master's degree from Zhengzhou University in 2007, and is currently an engineer at Shanghai Astronomy Observatory, China Academy of Sciences. Her current research focuses on quality management